

Recurrent Multi-Graph Neural Networks for Travel Cost Prediction

Jilin Hu, Chenjuan Guo, Bin Yang, Christian S. Jensen, Lu Chen
 Department of Computer Science, Aalborg University, Denmark
 {hujilin, cguo, byang, csj, luchen}@cs.aau.dk

ABSTRACT

Origin-destination (OD) matrices are often used in urban planning, where a city is partitioned into regions and an element (i, j) in an OD matrix records the cost (e.g., travel time, fuel consumption, or travel speed) from region i to region j . In this paper, we partition a day into multiple intervals, e.g., 96 15-min intervals and each interval is associated with an OD matrix which represents the costs in the interval; and we consider sparse and stochastic OD matrices, where the elements represent stochastic but not deterministic costs and some elements are missing due to lack of data between two regions.

We solve the sparse, stochastic OD matrix forecasting problem. Given a sequence of historical OD matrices that are sparse, we aim at predicting future OD matrices with no empty elements. We propose a generic learning framework to solve the problem by dealing with sparse matrices via matrix factorization and two graph convolutional neural networks and capturing temporal dynamics via recurrent neural network. Empirical studies using two taxi datasets from different countries verify the effectiveness of the proposed framework.

ACM Reference Format:

Jilin Hu, Chenjuan Guo, Bin Yang, Christian S. Jensen, Lu Chen, Department of Computer Science, Aalborg University, Denmark, {hujilin, cguo, byang, csj, luchen}@cs.aau.dk, .2018. Recurrent Multi-Graph Neural Networks for Travel Cost Prediction. In *Proceedings of ACM Conference (Conference'17)*. ACM, New York, NY, USA, 12 pages. <https://doi.org/10.1145/nnnnnnn.nnnnnnn>

1 INTRODUCTION

Origin-destination (OD) matrices [11, 18] are applied widely in location based services and online map services (e.g., transportation-as-a-service), where OD matrices are used for the scheduling of trips, for computing payments for completed trips, and for estimating arrival times. For example, Google Maps¹ and ESRI ArcGIS Online² offer OD matrix services to help developers to develop location based applications. Further, increased urbanization contributes to making it increasingly relevant to capture and study city-wide traffic conditions. OD matrices may also be applied for this purpose.

To use OD-matrices, a city is partitioned into *regions*, and a day is partitioned into *intervals*. Each interval is assigned its own an

¹<https://tinyurl.com/7vmtk4y>
²<https://tinyurl.com/ydhq765h>

Permission to make digital or hard copies of part or all of this work for personal or classroom use is granted without fee provided that copies are not made or distributed for profit or commercial advantage and that copies bear this notice and the full citation on the first page. Copyrights for third-party components of this work must be honored. For all other uses, contact the owner/author(s).

Conference'17, July 2017, Washington, DC, USA
 © 2018 Copyright held by the owner/author(s).
 ACM ISBN 978-x-xxxx-xxxx-x/YY/MM.
<https://doi.org/10.1145/nnnnnnn.nnnnnnn>



(a) Grid-based Partition

(b) Road-based Partition

Figure 1: Partition a City into Regions

OD-matrix, and an element (i, j) in matrix described the attribute (e.g., travel speed, fuel consumption [13, 14], or travel demand) of travel from region i to region j during the interval that the matrix represents. Different approaches can be applied to partition a road network [9, 48], e.g., using a uniform grid or using major roads, as exemplified in Figure 1. In this paper, we focus on speed matrices. However, the proposed techniques can be applied on other travel attributes or costs, such as travel time, fuel consumption, and travel demand.

As part of the increasing digitization of transportation, increasingly vast volumes of vehicle trajectory, trajectory data are becoming available [10, 12]. We aim to exploit such data for composing OD matrices. Specifically, an element (i, j) of a speed matrix for a given time interval can be instantiated from the speeds observed in trajectories that went from region i to region j during the relevant time interval.

We consider *stochastic OD matrices* where the elements represent uncertain costs by meaning of cost distributions rather than deterministic, single-valued costs. The use of distribution models reality better and enables more reliable decision-making. For example, element (i, j) has a speed histogram $\{([10, 20], 0.5), ([20, 40], 0.3), ([40, 60], 0.2)\}$, meaning that the probability of traveling speed from region i to region j at 0-20 km/h is 0.5, at [20, 30] is 0.3, and at [30, 40] is 0.2, respectively. If a passenger needs to go from his home in region i to catch a flight in an airport in region j , and the shortest path from his home to the airport is 20 km, then we are able to derive a travel time (minutes) distribution: $\{([30, 40], 0.5), (40, 60], 0.3), (60, 120], 0.2)\}$. Therefore, the passenger needs to reserve at least 120 minutes for not being late. However, when only using average speed to derive an average travel time of 54 minutes, it makes the passenger runs into a risk of missing the flight.

We address the problem of *stochastic origin-destination matrix forecasting*—based on historical stochastic OD-matrices, we predict future OD-matrices. Figure 2 shows a specific example: given

stochastic OD-matrices for 3 historical intervals $T^{(t-2)}$, $T^{(t-1)}$, and $T^{(t)}$, we aim at predicting the stochastic OD-matrices for the 3 future intervals $T^{(t+1)}$, $T^{(t+2)}$, and $T^{(t+3)}$.

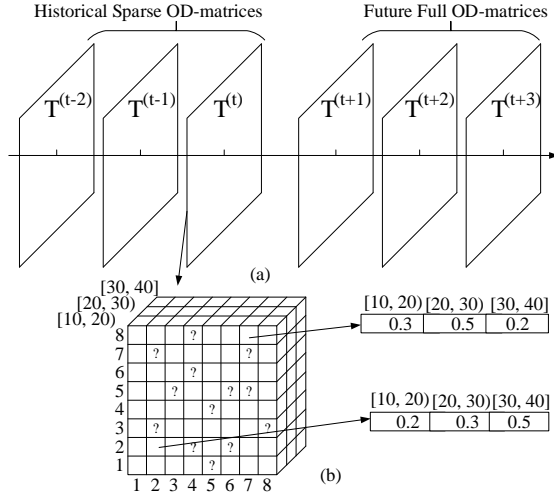


Figure 2: Stochastic Origin-Destination Matrix Forecasting

Here, a stochastic OD-matrix is represented as a 3-dimensional tensor, where the first dimension represents source regions, the second dimension represents destination regions, and the third dimension represents cost ranges. For example, Figure 2(b) shows the stochastic OD-matrix for interval $T^{(t)}$, which is represented as a $\mathcal{R}^{8 \times 8 \times 3}$ tensor with 8 source regions, 8 destination regions, and 3 speed (km/h) ranges $[10, 20]$, $[20, 30]$, and $[30, 40]$. Element (8, 8) in the OD-matrix is a vector (0.3, 0.5, 0.2), meaning that, when traveling within region 8, the travel speed histogram is $\{([10, 20], 0.3), ([20, 30], 0.5), ([30, 40], 0.2)\}$.

Solving the stochastic OD-matrix forecasting problem is non-trivial as it is necessary to contend with two difficult challenges.

(1) **Data Sparseness.** To instantiate a stochastic OD-matrix in an interval using trajectories, we need to have sufficient trajectories for each region pair during the interval. However, even massive trajectory data sets are often spatially and temporally skewed [15, 20, 39–41], making it almost impossible to cover all region pairs for all intervals.

For example, the New York City taxi data set³ we use in experiments has more than 29 million trips from November and December 2013. Yet, this massive trip set only covers 65% of all “taxizone” pairs in Manhattan, the most densely traversed region in New York City. If we further split the data set according to the temporal dimension, e.g., into 15-min intervals, the sparseness problem becomes even more severe.

The data sparseness in turn results in sparse historical stochastic OD-matrices, where some elements are empty (e.g., those elements with “?” in Figure 2(b)). Yet, decision making requires full OD-matrices. The challenge is how to use sparse historical OD-matrices to predict full future OD-matrices.

(2) **Spatio-temporal Correlations.** Traffic is often spatio-temporally correlated—if a region is congested during a time interval, its neighboring regions are also likely to be congested in subsequent intervals. Thus, to predict accurate OD-matrices, we need to account for such spatio-temporal correlations. However, the OD-matrices themselves do not necessarily capture spatial proximity. No matter which partition method is used, we cannot always guarantee that two geographically adjacent regions are represented by adjacent rows and columns in the matrix. For example, in Figure 1(a), regions 1 and 4 are geographically adjacent, but they are not adjacent in the OD matrices; in Figure 1(b), regions 4 and 7 are adjacent but they are again not adjacent in the OD matrices. This calls for a separate mechanism that is able to take into account the geographical proximity of regions.

We propose a data-driven, end-to-end deep learning framework to forecast stochastic OD matrices that aims to effectively address the challenges caused by data sparseness and spatio-temporal correlations. First, to address the data sparseness challenge, we factorize a sparse OD matrix into two small dense matrices with latent features of the source regions and the destination regions, respectively. Second, we model the spatial relationships among source regions and among destination regions using two graphs, respectively. Then, we employ two graph convolutional, recurrent neural networks (GR) on the two dense matrices to capture the spatio-temporal correlations. Finally, the two GRs predict two dense, small matrices. We apply the multiplication to the two dense, small matrices to obtain a full predicted OD-matrix.

To the best of our knowledge, this is the first study of stochastic OD matrix forecasting that contends with data sparseness and spatio-temporal correlations. The study makes four contributions. First, it formalizes the stochastic OD matrix forecasting problem. Second, it proposes a generic framework to solve the problem based on matrix factorization and recurrent neural networks. Third, it extends the framework by embedding spatial correlations using two graph convolutional neural networks. Fourth, it encompasses an extensive experiments using two real-world taxi datasets that offers insight into the effectiveness of the framework.

The remainder of the paper is organized as follows. Section 2 covers related works. Section 3 defines the setting and formalizes the problem. Section 4 introduces a basic framework and Section 5 presents an advanced framework. Section 6 reports experiments and Section 7 concludes.

2 RELATED WORK

2.1 Travel Cost Forecasting

We consider three types of travel cost forecasting methods in turn: segment-based methods [19, 30, 42, 44–46, 50], path-based methods [7, 38, 40, 41, 43, 52], and OD-based methods [20, 25, 39].

Segment-based methods focus on predicting the travel costs of individual road segments. For example, by modeling the travel costs of a road segment as a time series, techniques such as time-varying linear regression [30], Markov models [44, 50], and support vector regression [42] can be applied to predict future travel costs. Most such models consider time series from different edges independently. As an exception, the spatio-temporal Hidden Markov model [44] takes into account the correlations among the costs of different edges.

³http://www.nyc.gov/html/tlc/html/technology/raw_data.shtml

Some other studies focus on estimating high-resolution travel costs, such as uncertain costs [19, 45] and personalized costs [6, 46]. The data sparseness problem has also been studied—methods exist to estimate travel costs for segments without traffic data [17, 47].

Path-based methods focus on predicting the travel costs of paths. A naive approach is to predict the costs of the edges in a path and then aggregate the costs. However, this approach is inaccurate since it ignores the dependencies among the costs of different edges in paths [7, 40]. Other methods [7, 40, 43] use sub-trajectories to capture such dependencies and thus to provide more accurate travel costs for paths. In particular, the P_Ath-C_Entric (PACE) model is proposed to utilize sub-trajectories that may overlap to achieve the optimal accuracy [7, 43], whereas the other study only considers non-overlapping sub-trajectories [40]. A few studies propose variations of deep neural networks [38, 41, 52] to enable accurate travel-time prediction for paths.

Finally, OD-based methods aim at predicting the travel cost for given OD pairs. Our proposal falls into this category. A simple and efficient baseline [39] is to compute a weighted average over all historical trajectories that represent travel from the origin to the destination in an OD pair. However, it does not address data sparseness, which means that if no data is available for a given OD pair, it cannot provide a prediction. In contrast, our proposal is able to predict full OD-matrices without empty elements based on historical, sparse OD-matrices. A recent study [25] utilizes deep learning and multi-task learning to predict OD travel time while taking into account considers the road network topology and the paths used in the historical trajectories. However, path information may not always be available. An example is the New York taxi data set that we use in the experiments. This reduces the applicability of the model. In contrast, our proposal does not require path information. Further, existing proposals support only deterministic costs, while our proposal also supports stochastic costs.

2.2 Graph Convolutional Neural Network

Convolutional Neural Networks (CNNs) have been used successfully in the contexts of images [32], videos [24], speech [16], time series [5, 22], and trajectories [21], where the underlying data is represented as a matrix [2, 8]. For example, when representing an image as a matrix, nearby elements, e.g., pixels, share local features, e.g., represent parts of the same object. In contrast, in our setting, an OD-matrix may not satisfy the assumption that helps make CNNs work—two adjacent rows in an OD matrix may represent two geographically distant regions and may not share any features; and two separated rows in an OD matrix may represent geographically close regions that share many features.

Graph convolutional neural networks (GCNNs) [2, 8] aim to address this challenge. In particular, the geographical relationships among regions can be modeled as a graph, and GCNNs then take into account the graph while learning. One study [23] applies GCNNs to solve semi-supervised classification in the setting of citation networks and knowledge graphs. One study continues to study semi-supervised classification via dual graph convolutional networks [53]. Another study [49] constructs GCNNs together with a Recurrent Neural Network (RNN) to forecast traffic and one recent study [17] utilizes GCNNs to fill in travel time for edges without traffic data.

All the above studies consider a setting where only one dimension needs to be modeled as a graph. In contrast, in our study, both dimensions, i.e., the source region dimension and the destination region dimension, need to be modeled as two graphs. An additional, recent study focuses on so-called geomatrix completion which considers a similar setting where two dimensions need to be modeled as two graphs. It uses multi-graph neural networks [28] with RNNs. However, the RNNs in this study are utilized to perform iterations to approximate the geomatrix completion, not to capture temporal dynamics as in our study. To the best of our knowledge, our study is the first that constructs a learning framework involving dual-graph convolution and employing RNNs to forecast the future.

3 PRELIMINARIES

3.1 OD Stochastic Speed Tensor

A **trip** p is defined as a tuple $p = (o, d, t, l, \tau)$, where o, d denote an origin and a destination, t is a departure time, l represents the trip distance, and τ is the travel time of the trip. Given $p.l$ and $p.\tau$, we derive the average travel speed v of p . We use \mathbb{P} to denote a set of historical trips.

To capture the time-dependent traffic, we partition the time domain TI of interest, e.g., a day, into a number of time intervals, e.g., 96 15-min intervals. For each time interval $T_i \in TI$, we obtain the set of historical trips \mathbb{P}_{T_i} from \mathbb{P} whose departure times belong to time interval T_i , i.e., $\mathbb{P}_{T_i} = \{p_i | p_i.t \in T_i \wedge p_i \in \mathbb{P}\}$.

We further partition a city into M regions $\mathbb{V} = \{\mathbb{V}_1, \dots, \mathbb{V}_M\}$. An **Origin-Destination (OD) pair** is defined as a pair of regions $(\mathbb{V}_o, \mathbb{V}_d)$ where $1 \leq o, d, \leq M$.

Given a time interval T_i , two regions \mathbb{V}_o and \mathbb{V}_d , we obtain a trip set $\mathbb{P}_{T_i, \mathbb{V}_o, \mathbb{V}_d} = \{p_i | p_i.o \in \mathbb{V}_o \wedge p_i.d \in \mathbb{V}_d \wedge p_i.t \in T_i\}$, meaning that each trip in $\mathbb{P}_{T_i, \mathbb{V}_o, \mathbb{V}_d}$ starts from region \mathbb{V}_o , at a time in interval T_i , and ends at region \mathbb{V}_d .

Next, we construct an equi-width histogram $\mathbb{H}_{T_i, \mathbb{V}_o, \mathbb{V}_d}$ to record the stochastic speed of trips in $\mathbb{P}_{T_i, \mathbb{V}_o, \mathbb{V}_d}$. In particular, an equi-width histogram is a set of K bucket-probability pairs, i.e., $\mathbb{H}_{T_i, \mathbb{V}_o, \mathbb{V}_d} = \{(b_j, pr_j)\}$. A bucket $b_j = [v_s, v_e)$ represents the speed range from v_s to v_e , and all buckets have the same range size. Probability pr_j is the probability that the average speed of a trip falls into the range b_j . For example, the speed histogram $\{([0, 20), 0.5), ([20, 40), 0.3), ([40, 60), 0.2) \}$ for $\mathbb{P}_{T_i, \mathbb{V}_o, \mathbb{V}_d}$ means that the probabilities that the average speed (km/h) of a trip in $\mathbb{P}_{T_i, \mathbb{V}_o, \mathbb{V}_d}$ falls into $[0, 20)$, $[20, 40)$, and $[40, 60)$ are 0.5, 0.3, and 0.2, respectively.

Definition 3.1. Given a time interval T_i , an **OD stochastic speed tensor** is defined as a matrix $\mathbf{M}^{(i)} \in \mathbb{R}^{N \times N' \times K}$, where the first and second dimensions range over the origin and destination regions, respectively, and the third dimension ranges over the stochastic speeds. For generality, the origin and destination regions can be the same or can be different; thus the first and second dimensions have N and N' instances, respectively. The third dimension defines K speed buckets.

$M_{o,d,k}$ represents the element (o, d, k) of tensor $\mathbf{M}^{(i)} \in \mathbb{R}^{N \times N' \times K}$ and represents the probability of trips in $\mathbb{P}_{T_i, \mathbb{V}_o, \mathbb{V}_d}$ traveling at an average speed that falls into the k -th bucket.

Following the example in Figure 2(b), given a time interval T_i , for origin region 7 and destination region 8, we obtain a stochastic

speed of trips as a histogram, in which the first bucket records that the probability of trips, starting at region 7 during time interval T_i and ending at region 8, traveling at an average speed of $[5, 10)$ is 0.3.

As shown in Figure 2(b), not all cells have a histogram to capture the stochastic speed. Specifically, the cells with question marks have no histograms because no trip records are available for those cells, i.e., $\mathbb{P}_{T_i, \mathbb{V}_o, \mathbb{V}_d} = \emptyset$, so that $\mathbb{H}_{T_i, \mathbb{V}_o, \mathbb{V}_d} = \emptyset$. We refer to such tensor as **sparse OD stochastic speed tensor**.

Given a time interval T_i , we refer to a tensor where each cell has a stochastic speed $\mathbb{H}_{T_i, \mathbb{V}_o, \mathbb{V}_d}$ as a **full OD stochastic speed tensor**.

3.2 Problem Definition

Given s sparse OD stochastic speed tensors $\mathbf{M}^{(t-s+1)}, \dots, \mathbf{M}^{(t)}$ during s historical time intervals $T^{(t-s+1)}, \dots, T^{(t)}$, we aim to predict the stochastic speeds for the next h time intervals $T^{(t+1)}, \dots, T^{(t+h)}$ in the form of h full OD stochastic speed tensors $\mathbf{M}^{(t+1)}, \dots, \mathbf{M}^{(t+h)}$ by learning the following function f .

$$f : [\mathbf{M}^{(t-s+1)}, \dots, \mathbf{M}^{(t)}] \rightarrow [\mathbf{M}^{(t+1)}, \dots, \mathbf{M}^{(t+h)}]$$

4 BASIC STOCHASTIC SPEED FORECASTING

4.1 Framework and Intuition

Figure 3 shows the basic framework for forecasting stochastic speeds, which consists of three steps: *Factorization*, *Forecasting*, and *Recovery*.

For the historical time intervals $T^{(t-s+1)}, \dots, T^{(t)}$, we have sparse OD stochastic speed tensors $\mathbf{M}^{(t-s+1)}, \dots, \mathbf{M}^{(t)}$. We factorize each stochastic speed tensor $\mathbf{M}^{(t-i+1)} \in \mathbb{R}^{N \times N' \times K}$, where $i \in [1, s]$ into two smaller tensors $\mathbf{R}^{(t-i+1)} \in \mathbb{R}^{N \times \beta \times K}$ and $\mathbf{C}^{(t-i+1)} \in \mathbb{R}^{\beta \times N' \times K}$, where $\beta \ll N, N'$. The aim is to use $\mathbf{R}^{(t-i+1)}$ and $\mathbf{C}^{(t-i+1)}$ to approximate $\mathbf{M}^{(t-i+1)}$. Here $\mathbf{R}^{(t-i+1)}$ and $\mathbf{C}^{(t-i+1)}$ model the correlated features of stochastic speeds among origin regions and among destination regions, respectively. And it is intuitive to assume that stochastic speeds among origin regions and among destination regions share correlated features, as traffic in a region affects the traffic in its nearby regions.

The factorization is supported by the intuition underlying low-rank matrix approximation [27, 28, 34, 35]. Since $\mathbf{M}^{(t-i+1)}$ is a sparse tensor, we aim to find a low-rank tensor $\mathbf{M}'^{(t-i+1)}$ to approximate $\mathbf{M}^{(t-i+1)}$. When carrying out the approximation, we assume that the rank of $\mathbf{M}^{(t-i+1)}$ is at most β and that it can be factorized as $\mathbf{M}^{(t-i+1)} = \mathbf{R}^{(t-i+1)} \times \mathbf{C}^{(t-i+1)}$. Then, the problem of using $\mathbf{M}'^{(t-i+1)}$ to approximate $\mathbf{M}^{(t-i+1)}$ can be formulated as the problem of minimizing the following loss function.

$$\min_{\mathbf{R}^{(x)}, \mathbf{C}^{(x)}} \|\mathbf{R}^{(x)}\|_F^2 + \|\mathbf{C}^{(x)}\|_F^2 + \frac{\mu}{2} \|\Omega \circ (\mathbf{R}^{(x)} \mathbf{C}^{(x)} - \mathbf{M}^{(x)})\|_F^2, \quad (1)$$

where $x = t - i + 1$, $\|\cdot\|_F$ denotes the Frobenius norm, $\Omega_{o,d,k}^{(x)} = 1$ if the element (o, d) of $M^{(x)}$ is not empty, and \circ is the element-wise tensor multiplication.

Next, we consider $\mathbf{R}^{(t-s+1)}, \dots, \mathbf{R}^{(t)}$ as an input sequence, from which we capture the temporal correlations among the origin regions

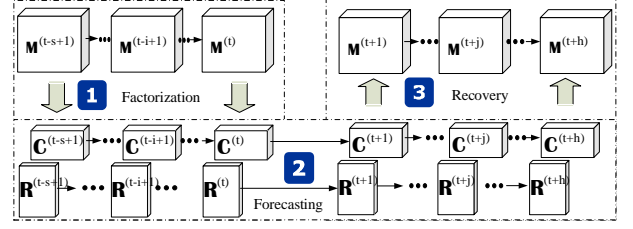


Figure 3: Framework Overview.

of $\mathbf{M}^{(t-s+1)}, \dots, \mathbf{M}^{(t)}$. We feed this input sequence into a sequence-to-sequence RNN model [36] to *forecast* an output sequence that represents the shared features among the origin regions in the future.

We apply a similar procedure to $\mathbf{C}^{(t+1)}, \dots, \mathbf{C}^{(t+h)}$ to *forecast* an output sequence that represents the shared features among destination regions in the future.

Finally, we *recover* $\mathbf{M}^{(t+j)}$ as a full OD stochastic speed tensor from $\mathbf{R}^{(t+j)}$ and $\mathbf{C}^{(t+j)}$, $j \in [1, h]$. Since we obtain the predictions $\mathbf{R}^{(t+j)}$ and $\mathbf{C}^{(t+j)}$ from the historical $\mathbf{R}^{(t-i+1)}$ and $\mathbf{C}^{(t-i+1)}$, $i \in [1, s]$, the intuition of Equation 1 also applies when reconstructing $\mathbf{M}^{(t+j)}$.

4.2 Factorization

Given an input sparse OD stochastic tensors $\mathbf{M}^{(t-i+1)} \in \mathbb{R}^{N \times N' \times K}$ for intervals $T^{(t-i+1)}$, where $i \in [1, s]$, we proceed to describe the method for factorizing $\mathbf{M}^{(t-i+1)}$ into $\mathbf{R}^{(t-i+1)}$ and $\mathbf{C}^{(t-i+1)}$, which are able to capture the correlated features of stochastic speed among origin and destination regions, respectively. We first flatten $\mathbf{M}^{(t-i+1)}$ into a vector $\mathbf{f}^{(t-i+1)} \in \mathbb{R}^l$, where $l = N \cdot N' \cdot K$, from which we generate two small factorization vectors, $\mathbf{c}^{(t-i+1)} \in \mathbb{R}^{N' \cdot K \cdot \beta}$ and $\mathbf{r}^{(t-i+1)} \in \mathbb{R}^{N \cdot K \cdot \beta}$ via a fully-connected neural network layer (FC layer).

$$\mathbf{r}^{(t-i+1)} = \text{relu}(\mathbf{F}_r \times \mathbf{f}^{(t-i+1)} + \mathbf{b}_r) \quad (2)$$

$$\mathbf{c}^{(t-i+1)} = \text{relu}(\mathbf{F}_c \times \mathbf{f}^{(t-i+1)} + \mathbf{b}_c) \quad (3)$$

Here $\mathbf{F}_r \in \mathbb{R}^{(N \cdot K \cdot \beta) \times l}$ and $\mathbf{F}_c \in \mathbb{R}^{(N' \cdot K \cdot \beta) \times l}$ are parameter matrices, where β is a hyper-parameter to be set; $\mathbf{b}_r \in \mathbb{R}^{(N \cdot K \cdot \beta)}$ and $\mathbf{b}_c \in \mathbb{R}^{(N' \cdot K \cdot \beta)}$ are bias vectors; and $\text{relu}(\cdot)$ is the relu activation function.

Next, we reorganize the factorization vectors $\mathbf{r}^{(t-i+1)}$ and $\mathbf{c}^{(t-i+1)}$ into factorization tensors $\mathbf{R}^{(t-i+1)} \in \mathbb{R}^{N \times \beta \times K}$ and $\mathbf{C}^{(t-i+1)} \in \mathbb{R}^{\beta \times N' \times K}$, respectively.

4.3 Forecasting

Given historical time intervals $T^{(t-s+1)}, \dots, T^{(t)}$, we learn the temporal correlations of $\mathbf{M}^{(t-s+1)}, \dots, \mathbf{M}^{(t)}$ from the temporal correlations among origin regions $\mathbf{R}^{(t-s+1)}, \dots, \mathbf{R}^{(t)}$ and the temporal correlation among destination regions $\mathbf{C}^{(t-s+1)}, \dots, \mathbf{C}^{(t)}$.

Based on $\mathbf{R}^{(t-s+1)}, \dots, \mathbf{R}^{(t)}$, we use a sequence-to-sequence RNN model [36] to forecast $\widehat{\mathbf{R}}^{(t+1)}, \dots, \widehat{\mathbf{R}}^{(t+h)}$ for the future time intervals T_{t+1}, \dots, T_{t+h} . In particular, we apply Gated Recurrent Units (GRUs) in the RNN architecture, since these can capture temporal correlations well by using gate units well and also offer high

efficiency [3, 4]. The process is presented as follows.

$$\widehat{\mathbf{R}}^{(t+1)}, \dots, \widehat{\mathbf{R}}^{(t+h)} = \text{seq2seqGRU}(\mathbf{R}^{(t-s+1)}, \dots, \mathbf{R}^{(t)}). \quad (4)$$

A similar procedure is applied to obtain $\widehat{\mathbf{C}}^{(t+1)}, \dots, \widehat{\mathbf{C}}^{(t+h)}$ from $\mathbf{C}^{(t-s+1)}, \dots, \mathbf{C}^{(t)}$.

4.4 Recovery

Given predicted tensors $\widehat{\mathbf{R}}^{(t+j)} \in \mathbb{R}^{N \times \beta \times K}$ and $\widehat{\mathbf{C}}^{(t+j)} \in \mathbb{R}^{\beta \times N' \times K}$ for a future time interval $T^{(t+j)}$, with $j \in [1, h]$, we proceed to describe how to transform $\widehat{\mathbf{R}}^{(t+j)}$ and $\widehat{\mathbf{C}}^{(t+j)}$ into a full OD stochastic speed tensor $\mathbf{M}^{(t+j)} \in \mathbb{R}^{N \times N' \times K}$.

First, we slice each of $\widehat{\mathbf{R}}^{(t+j)}$ and $\widehat{\mathbf{C}}^{(t+j)}$ by the speed bucket dimension into K matrices. Specifically, we have $\text{slice}(\widehat{\mathbf{R}}^{(t+j)}) = \{\widehat{\mathbf{R}}_{\cdot, \cdot, 1}^{(t+j)} \dots, \widehat{\mathbf{R}}_{\cdot, \cdot, K}^{(t+j)}\}$ and $\text{slice}(\widehat{\mathbf{C}}^{(t+j)}) = \{\widehat{\mathbf{C}}_{\cdot, \cdot, 1}^{(t+j)} \dots, \widehat{\mathbf{C}}_{\cdot, \cdot, K}^{(t+j)}\}$, where $\widehat{\mathbf{R}}_{\cdot, \cdot, k}^{(t+j)} \in \mathbb{R}^{N \times \beta}$ and $\widehat{\mathbf{C}}_{\cdot, \cdot, k}^{(t+j)} \in \mathbb{R}^{\beta \times N'}$, $k \in [1, K]$.

Next, we conduct a matrix multiplication as follows.

$$\widetilde{\mathbf{M}}_k^{(t+j)} = \widehat{\mathbf{R}}_{\cdot, \cdot, k}^{(t+j)} \times (\widehat{\mathbf{C}}_{\cdot, \cdot, k}^{(t+j)}), \quad (5)$$

where $\widetilde{\mathbf{M}}_k^{(t+j)} \in \mathbb{R}^{N \times N'}$, $k \in [1, K]$.

Finally, we are able to construct a tensor $\widetilde{\mathbf{M}}^{(t+j)} \in \mathbb{R}^{N \times N' \times K}$ by combining a total of K matrices, i.e., $\widetilde{\mathbf{M}}_{\cdot, \cdot, k}^{(t+j)} = \widetilde{\mathbf{M}}_k^{(t+j)}$, $k \in [1, K]$. Now, $\widetilde{\mathbf{M}}^{(t+j)}$ is a full tensor where each element has a value.

A histogram $\widehat{\mathbf{M}}_{o, d, \cdot}^{(t+j)} \in \mathbb{R}^{1 \times K}$ must meet two requirements to be a meaningful histogram: (1) $\widehat{\mathbf{M}}_{o, d, k}^{(t+j)} \in [0, 1]$, $k \in [1, K]$, meaning that the probability of a speed falling into the k -th bucket for each OD pair (o, d) must be between 0 and 1; and (2) $\sum_{k=1}^K \widehat{\mathbf{M}}_{o, d, k}^{(t+j)} = 1$, meaning that the probability of a speed falling into all K buckets for each (o, d) must equal 1.

To achieve this, we apply a softmax function to normalize values in $\widetilde{\mathbf{M}}^{(t+j)}$ into $\widehat{\mathbf{M}}_{o, d, \cdot}^{(t+j)}$ that satisfies the histogram requirements.

$$\widehat{\mathbf{M}}_{o, d, \cdot}^{(t+j)} = \text{softmax}(\widetilde{\mathbf{M}}_{o, d, \cdot}^{(t+j)}), \forall o \in [1, N], \forall d \in [1, N']. \quad (6)$$

Thus, we obtain h meaningful full OD stochastic speed tensors for the future time intervals T_{t+1}, \dots, T_{t+h} as the output of the recovery process: $\widehat{\mathbf{M}}^{(t+1)}, \dots, \widehat{\mathbf{M}}^{(t+h)}$.

4.5 Loss Function

The loss function is defined as the error between the recovered future tensor and the ground-truth future tensor.

$$\begin{aligned} \ell(F, \mathbf{b}) = & \sum_{j=1}^h [\lambda \|\widehat{\mathbf{R}}^{(t+j)}\|_F^2 + \lambda \|\widehat{\mathbf{C}}^{(t+j)}\|_F^2 + \\ & \|\Omega^{(t+j)} \circ (\mathbf{M}^{(t+j)} - \widehat{\mathbf{M}}^{(t+j)})\|_F^2], \end{aligned} \quad (7)$$

where F and \mathbf{b} represent the training parameters in the framework, and λ is a regularization parameter. Further, $\Omega^{(t+j)} \in \mathbb{R}^{N \times N' \times K}$ is an indication tensor, where $\Omega_{o, d, k}^{(t+j)} = 1$ if the OD pair (o, d) is not empty in the $t+j$ 'th future interval. Note that although we aim to predict full tensors, the ground truth tensors are sparse, so we compute the errors

taking only into account the non-empty elements in the ground truth tensors. Next, \circ is element-wise multiplication, $\widehat{\mathbf{M}}^{(t+j)}$ and $\mathbf{M}^{(t+j)}$ are predicted and ground truth tensors, respectively, $\|\cdot\|_F$ is the Frobenius-norm.

5 FORECAST WITH SPATIAL DEPENDENCY

To improve forecast accuracy, we proceed to integrate spatial dependency into our framework in two different stages. First, in the factorization step, we apply graph convolutional neural networks to perform feature encoding for origin and destination dimensions, respectively. Second, in the forecasting step, we integrate graph convolutional with RNNs to capture spatio-temporal correlations.

5.1 Spatial Factorization

As in Section 4.2, we aim to factorize tensor $\mathbf{M}^{(t-i+1)}$ during interval T_{t-i+1} , $i \in [1, s]$, into two smaller tensors $\mathbf{C}^{(t-i+1)}$ and $\mathbf{R}^{(t-i+1)}$. In Section 4.2, $\mathbf{M}^{(t-i+1)}$ is simply flattened and followed by a fully-connected layer to construct $\mathbf{C}^{(t-i+1)}$ and $\mathbf{R}^{(t-i+1)}$. This process does not take spatial correlations among the origin regions and among the destination regions into account, although such correlations are likely to exist. To accommodate spatial correlations, we first capture spatial correlations among origin and destination regions; then we use the captured spatial correlations to conduct factorization.

5.1.1 Spatial Correlation. We leverage the notion of a proximity matrix [26] to capture spatial correlations. We proceed to present the idea using origin regions as an example, which also applies to destination regions in a similar manner.

Given $\mathbf{M}^{(t-i+1)} \in \mathbb{R}^{N \times N' \times K}$, we have N origin regions, from which we build an adjacency matrix $\mathbf{A} \in \mathbb{R}^{N \times N}$ to show region connections. Specifically, $\mathbf{A}_{u, v} = 1$ means that regions \mathbb{V}_u and \mathbb{V}_v are adjacent; otherwise, $\mathbf{A}_{u, v} = 0$.

We construct a weighted proximity matrix $\mathbf{W}^{(\alpha, \sigma)} \in \mathbb{R}^{N \times N}$ from \mathbf{A} that describes the proximity between regions \mathbb{V}_u and \mathbb{V}_v and is parameterized by adjacency hops α and standard deviation σ . Specifically, if \mathbb{V}_v can be reached from \mathbb{V}_u in α adjacency hops using \mathbf{A} , $\mathbf{W}_{u, v}^{(\alpha, \sigma)} = e^{-x^2/\sigma^2}$, where x is the distance between the centroid of \mathbb{V}_u and \mathbb{V}_v ; otherwise $\mathbf{W}_{u, v}^{(\alpha, \sigma)} = 0$. In the experiments, we study the effect of α and σ (see Section 6.2.4). The proximity matrix $\mathbf{W}^{(\alpha, \sigma)}$ is symmetric and non-negative.

The adjacency matrices for the source regions and destination regions may be different or the same. Consider two scenarios. First, we use OD matrices to model the travel costs within a city. In this case, the source regions and the destination regions are the same, and thus the two adjacency matrices are the same. Second, we may use OD matrices to model the travel costs between two different cities. Then, the source regions and the destination regions are in different cities. Thus, we need two different adjacency matrices. To avoid confusion, we use \mathbf{W} and \mathbf{W}' represent the adjacency matrices for source regions and destination regions, respectively.

5.1.2 Factorization. We proceed to show the factorization procedure. Specifically, we show how to obtain $\mathbf{R}^{(t-i+1)}$ from $\mathbf{M}^{(t-i+1)}$. The same procedure can be applied to obtain $\mathbf{C}^{(t-i+1)}$.

As shown in Figure 4(a), we first slice $\mathbf{M}^{(t-i+1)} \in \mathbb{R}^{N \times N' \times K}$ by the origin region dimension into N matrices, i.e., $\text{slice}(\mathbf{M}^{(t-i+1)}) =$

$[\mathbf{M}_{1,:}^{(t-i+1)}, \dots, \mathbf{M}_{N,:}^{(t-i+1)}]$. Each of the sliced matrix is then applied with a GCNN operation. Accordingly, we obtain the GCNN output as $[\mathbf{R}_{1,:}^{(t-i+1)}, \dots, \mathbf{R}_{N,:}^{(t-i+1)}]$. We then concatenate this to obtain $\mathbf{R}^{(t-i+1)} \in \mathbb{R}^{N \times \beta' \times K}$.

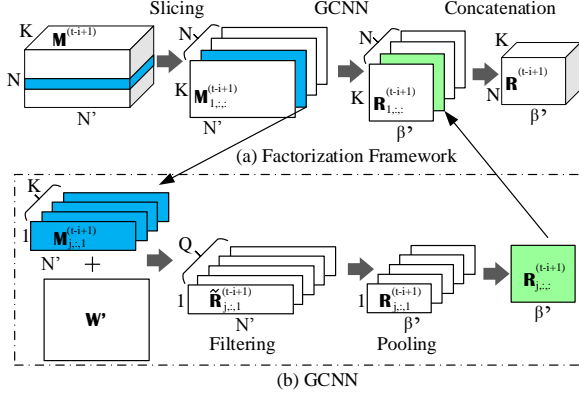


Figure 4: Spatial Factorization for R

Figure 4(b) shows a GCNN operation on a sliced matrix $\mathbf{M}_{j,:}^{(t-i+1)}$, $j \in [1, N]$, which transforms $\mathbf{M}_{j,:}^{(t-i+1)} \in \mathbb{R}^{K \times N'}$ into $\mathbf{R}_{j,:}^{(t-i+1)} \in \mathbb{R}^{K \times \beta'}$ via *Filtering* and *Pooling*.

Filtering: Given $\mathbf{M}_{j,:}^{(t-i+1)} \in \mathbb{R}^{K \times N'}$, we apply Q graph convolutional filters, which take into account the destination region adjacency matrix W , to generate $\tilde{\mathbf{R}}_{j,:}^{(t-i+1)} \in \mathbb{R}^{N' \times Q}$ that captures the correlated features among destination regions.

We first slice $\mathbf{M}_{j,:}^{(t-i+1)} \in \mathbb{R}^{K \times N'}$ into K vectors $[\mathbf{M}_{j,:1}^{(t-i+1)}, \dots, \mathbf{M}_{j,:K}^{(t-i+1)}]$, where vector $\mathbf{M}_{j,:k}^{(t-i+1)} \in \mathbb{R}^{N'}$, $k \in [1, K]$, represents the probability of speeds falling into the k -th speed bucket when traveling from origin region \forall_j to all destination regions.

Next, we use a specific graph convolutional filter, namely Cheby-Net [8], due to its high accuracy and efficiency, on each vector $\mathbf{M}_{j,:k}^{(t-i+1)}$. Specifically, before conducting actual convolutions, we compute $T_k^{(t-i+1)} = [t_1, t_2, \dots, t_S]$, where $t_s \in \mathbb{R}^{N'}$, $s \in [1, S]$, from $\mathbf{M}_{j,:k}^{(t-i+1)}$. Here, $t_1 = \mathbf{M}_{j,:k}^{(t-i+1)}$, $t_2 = \hat{L} \times \mathbf{M}_{j,:k}^{(t-i+1)}$, and $T_s = 2\hat{L} \times T_{s-1} - T_{s-2}$ when $s > 2$, where $\hat{L} = 2L/\lambda_{max} - I$ is a scaled Laplacian matrix and where $L = D - W'$ is the Laplacian matrix and λ_{max} is the maximum eigenvalue of L . Here, we use destination adjacency matrix W' because $\mathbf{M}_{j,:k}^{(t-i+1)}$ represents the speed from source region j to all destination regions and we use W' to capture the spatial correlation among destination regions. After the whole computation, we get $T_k \in \mathbb{R}^{N' \times S}$ as the encoded features for the k -th bucket while considering the spatial correlations among destination regions.

Then we proceed to apply Q filters to T_k . Each filter is a vector $\mathbf{G}_q \in \mathbb{R}^S$, where $q \in [1, Q]$. We apply each filter to all $\{T_k^{(t-i+1)}\}$,

$\forall k \in [1, K]$, and then the sum is used as the output of the filter.

$$\tilde{\mathbf{R}}_{j,:}^{(t-i+1)} = \mathbf{G}_q \otimes \mathbf{M}_{j,:}^{(t-i+1)} = \sum_{k=1}^K (\epsilon(T_k^{(t-i+1)} \times \mathbf{G}_q + b_q), \quad (8)$$

where \otimes is the Cheby-Net graph convolution operation, $b_q \in \mathbb{R}^{N'}$ is a bias vector, and $\epsilon(\cdot)$ is a non-linear activate function.

Finally, we arrange the results obtained from all Q filters as $\tilde{\mathbf{R}}_{j,:}^{(t-i+1)} = [\tilde{\mathbf{R}}_{j,:1}^{(t-i+1)}, \dots, \tilde{\mathbf{R}}_{j,:Q}^{(t-i+1)}]$, where $\tilde{\mathbf{R}}_{j,:}^{(t-i+1)} \in \mathbb{R}^{Q \times N'}$.

Pooling: To further condense the features and to construct the final factorizations, we apply geometrical pooling [8] to $\tilde{\mathbf{R}}_{j,:}^{(t-i+1)}$ over the destination region dimension to obtain $\mathbf{R}_{j,:}^{(t-i+1)} \in \mathbb{R}^{Q \times \beta'}$, where $\beta' = \frac{N'}{p}$ and p are the pooling and stride size, respectively. This process is shown as follows.

$$\mathbf{R}_{j,:}^{(t-i+1)} = P(\tilde{\mathbf{R}}_{j,:}^{(t-i+1)}), \quad (9)$$

where $P(\cdot)$ is the pooling function that can be either max pooling or average pooling.

Since the pooling operation requires meaningful neighborhood relationships, we identify spatial clusters of destination regions. For example, in Figure 1(b), if we use the order of ascending region ids, i.e., (1, 2, 3, 4, 5, 6, 7, 8) to conduct pooling with a pooling size of 2, then regions 3 and 4 are pooled together. However, regions 3 and 4 are not neighbors, so this procedure may yield inferior features that may in turn yield undesired results. Instead, if we identify clusters of regions, we are able to produce a new order, e.g., (6, 1, 2, 3, 5, 4, 7, 8). When again using a pooling size of 2, each pool contains neighbouring regions.

The GCNN process, including filtering and pooling, is repeated several times with different numbers of filters Q and pooling stride size p . Eventually, we set $Q = K$ and get $\mathbf{R}_{j,:}^{(t-i+1)} \in \mathbb{R}^{\beta' \times K}$.

As shown in Figure 4(b), the last operation is concatenation. We slice $\mathbf{M}^{(t-i+1)}$ by the origin region dimension into N matrices $[\mathbf{M}_{1,:}^{(t-i+1)}, \dots, \mathbf{M}_{N,:}^{(t-i+1)}]$ and apply GCNN to each of them to obtain $[\mathbf{R}_{1,:}^{(t-i+1)}, \dots, \mathbf{R}_{N,:}^{(t-i+1)}]$, where each $\mathbf{R}_{j,:}^{(t-i+1)} \in \mathbb{R}^{\beta' \times K}$. We then concatenate the $\mathbf{R}_{j,:}^{(t-i+1)}$, $j \in [1, N]$, to obtain $\mathbf{R}^{(t-i+1)} \in \mathbb{R}^{N \times \beta' \times K}$.

The same procedure can be applied to obtain $\mathbf{C}^{(t-i+1)}$ where we need to change W' to W when conducting the graph convolution.

5.2 Spatial Forecasting

To model temporal dynamics while keeping the spatial correlations in RNNs, we combine Cheby-Net based graph convolution with RNNs, yielding CNRNNs. Intuitively, we follow the structure of gated recurrent units while replacing the traditional fully connected layer by a Cheby-Net based graph convolution layer. Separate CNRNNs are employed to process $\mathbf{R}^{(t)}$ and $\mathbf{C}^{(t)}$.

Taking the source region dimension as an example, a CNRNN takes as input $\mathbf{R}^{(t)}$ at time interval $T^{(t)}$, and it predicts $\hat{\mathbf{R}}^{(t+1)}$ for the

future time interval $T^{(t+1)}$. This procedure is formulated as follows.

$$\mathbf{S}^{(t+1)} = \sigma(\mathbf{G}_S \otimes [\mathbf{H}^{(t)} : \mathbf{R}^{(t)}] + \mathbf{b}_S) \quad (10)$$

$$\mathbf{U}^{(t+1)} = \sigma(\mathbf{G}_U \otimes [\mathbf{H}^{(t)} : \mathbf{R}^{(t)}] + \mathbf{b}_U) \quad (11)$$

$$\mathbf{H}^{(t+1)} = \tanh(\mathbf{G}_H \otimes [\mathbf{R}^{(t)} : (\mathbf{S}^{(t+1)} \circ \mathbf{H}^{(t)})] + \mathbf{b}_H) \quad (12)$$

$$\widehat{\mathbf{R}}^{(t+1)} = \mathbf{U}^{(t+1)} \circ \mathbf{R}^{(t)} + (1 - \mathbf{U}^{(t+1)}) \circ \mathbf{H}^{(t+1)} \quad (13)$$

where \mathbf{G}_S , \mathbf{G}_U , and \mathbf{G}_H are graph convolution filters; $\mathbf{R}^{(t)}$ and $\widehat{\mathbf{R}}^{(t+1)}$ are the input and output of a CNRNN cell at time interval $T^{(t)}$, respectively; $\mathbf{S}^{(t)}$ and $\mathbf{U}^{(t)}$ are the reset and update gates, respectively; \otimes denotes the graph convolution which defined in Equation 8, and here the graph convolution should take into account source adjacency matrix \mathbf{W} since \mathbf{R} captures features of source regions. \circ denotes the Hadamard product between two tensors; and $\epsilon(\cdot)$, $\sigma(\cdot)$, and $\tanh(\cdot)$ are non-linear activation functions.

When applying CNRNN to predict $\widehat{\mathbf{C}}^{(t+1)}$, we need to change \mathbf{W} to \mathbf{W}' when conducting the graph convolution as \mathbf{R} captures features of destination regions.

Given predicted factorization tensors $[\widehat{\mathbf{R}}^{(t+1)}, \dots, \widehat{\mathbf{R}}^{(t+h)}]$ and $[\widehat{\mathbf{C}}^{(t+1)}, \dots, \widehat{\mathbf{C}}^{(t+h)}]$, we apply the same recovery operation introduced in Section 4.4 to obtain h full OD stochastic speed tensors for the future time intervals $T^{(t+1)}, \dots, T^{(t+h)}$ as the recovery output: $\widehat{\mathbf{M}}^{(t+1)}, \dots, \widehat{\mathbf{M}}^{(t+h)}$.

5.3 Loss Function

Similar to the construction covered in Section 4.5, we present the loss function as follows.

$$\ell(\mathbf{G}, \mathbf{b}) = \sum_{i=1}^h [\lambda \|\mathbf{R}^{(t+i)}\|_{\mathbf{W}}^2 + \lambda \|\mathbf{C}^{(t+i)}\|_{\mathbf{W}}^2 + \|\Omega^{(t+i)} \circ (\mathbf{M}^{(t+i)} - \widehat{\mathbf{M}}^{(t+i)})\|_{\mathbf{F}}^2] \quad (14)$$

where \mathbf{G} and \mathbf{b} represent the training parameters in the framework (in particular, graph convolutional filters and bias vectors), $\|\cdot\|_{\mathbf{W}}^2$ is the Dirichlet norm under the proximity matrix \mathbf{W} , λ is the regularization parameter for the Dirichlet norm. We use the Dirichlet norm because it takes the adjacency matrix into account—nearby regions should share similar features in the dense tensors \mathbf{R} and \mathbf{C} . Finally $\Omega^{(t+i)} \in \mathbb{R}^{N \times N' \times K}$ is an indication tensor, and $\widehat{\mathbf{M}}^{(t+i)}$ and $\mathbf{M}^{(t+i)}$, $j \in [1, h]$, are the predicted and ground truth tensors, respectively.

6 EXPERIMENTS

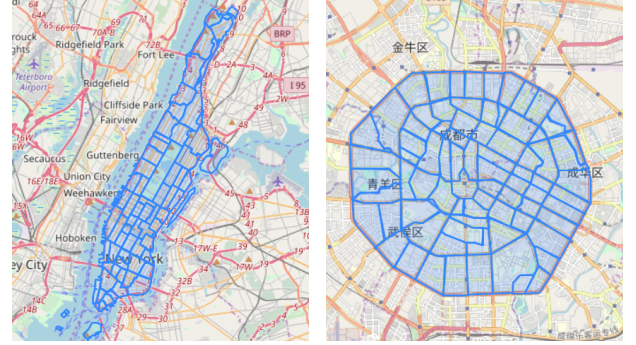
We describe the experimental setup and then present the experiments and the findings.

6.1 Experimental Setup

6.1.1 Datasets. We conduct experiments on two taxi trip datasets to study the effectiveness of the proposal.

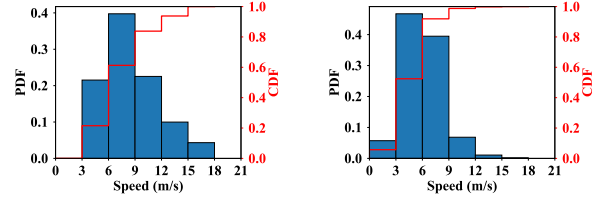
We represent a stochastic speed (m/s) as a histogram with 7 buckets $[0, 3)$, $[3, 6)$, $[6, 9)$, $[9, 12)$, $[12, 15)$, $[15, 18)$, and $[18, \infty)$; and we consider 15-min intervals, thus obtaining 96 15-min intervals per day.

New York City Data Set (NYC): We use 14 million taxi trips collected from 2013-11-01 to 2013-12-31 from Manhattan, New



(a) NYC Regions

(b) CD Regions



(c) NYC Speed

(d) CD Speed

Figure 5: Region Representations of NYC and CD

| | NYC | CD |
|---------------|------------|-----------|
| # Trips | 14,165,748 | 3,636,845 |
| # Regions | 67 | 79 |
| Average Speed | 8.8 m/s | 6.0 m/s |

Table 1: Statistics of the Data Sets.

York City. Each trip consists of a pickup time, a drop off time, a pickup location, a drop off location, and a total distance. Manhattan has 67 taxizones⁴, each of which is used as a region. The regions are shown in Figure 5(a). The OD stochastic speeds for NYC are represented as an $\mathbb{R}^{67 \times 67 \times 7}$ tensor.

Chengdu Data Set (CD): CD contains 1.4 billion GPS records from 14,864 taxis collected from 2014-08-03 to 2014-08-30 in Chengdu, China⁵. Each GPS record consists of a taxi ID, a latitude, a longitude, an indicator of whether the taxi is occupied, and a timestamp. We consider sequences of GPS records where taxis were occupied as trips. We use a total of 3,636,845 trips that occurred within the second ring road of Chengdu. Next, we partition Chengdu within the second ring road into 79 regions according to the main roads; see Figure 5(b). The OD stochastic speeds for CD are represented as an $\mathbb{R}^{79 \times 79 \times 7}$ tensor.

Table 1 shows the statistics of the two datasets. Figures 5(d) and 5(d) show the speed distributions for both datasets. We use 70% of the data for training, 10% for validation, and the remaining 20% for testing for both NYC and CD.

⁴http://www.nyc.gov/html/tlc/html/about/trip_record_data.shtml

⁵<https://goo.gl/3VsEym>

6.1.2 Forecast Settings. We consider settings where $s = 3$ or $s = 6$ while varying h among 1, 2, and 3. This means that we use stochastic OD matrices from 3 or 6 historical intervals to predict stochastic OD matrices during up to 3 future intervals, respectively. An example for $s = 6$ and $h = 3$ can be: given stochastic OD matrices in intervals [8:00, 8:15), [8:15, 8:30), [8:30, 8:45), [8:45, 9:00), [9:00, 9:15), and [9:15, 9:30), we predict stochastic OD matrices in intervals [9:30, 9:45), [9:45, 10:00), and [10:00, 10:15).

6.1.3 Baselines. To evaluate the effectiveness of the proposed base framework (BF) and the advanced framework (AF), we consider five baselines. (1) Naive Histograms (NH): for each OD pair, we use all travel speed records for the OD pair in the training data set to construct a histogram and use the histogram for predicting the future stochastic speeds. Next, we model the stochastic speeds for each OD pair as a time series of vectors, where each vector represents the stochastic speed of the OD pair in an interval. Based on this time series modeling, we consider three time series forecasting methods: (2) Support Vector Regression (SVR) [1], (3) Vector Autoregression (VAR) [33], and (4) Gaussian Process Regression (GP) [29]. (5) Fully Connected (FC): this is a variant of BF where we only directly use a fully connected layer to obtain a single dense tensor (instead of performing factorization into two dense tensors) to replace the factorization step in BF.

6.1.4 Evaluation Metrics. To quantify the effectiveness of the proposed frameworks, we use three commonly used distance functions that work for distributions, i.e., Kullback-Leibler divergence (KL), Jensen-Shannon divergence (JS), and earth-mover's distance (EMD), to measure the accuracy of forecasts.

Specifically, the general dissimilarity metric is defined as follows.

$$\text{DisSim}_{\text{metric}}^{(k)} = \frac{\sum_{t=1}^T \sum_{i=1}^N \sum_{j=1}^{N'} \Omega_{i,j}^{(t+k)} \text{metric}(\mathbf{M}_{i,j,:}^{(t+k)}, \widehat{\mathbf{M}}_{i,j,:}^{(t+k)})}{\sum_{t=1}^T \sum_{i=1}^N \sum_{j=1}^N \Omega_{i,j}^{(t+k)}}, \quad (15)$$

where $1 \leq k \leq h$ denotes the k -th step ahead forecasts, T is the size of testing set. Next, $\Omega_{i,j}^{(t+k)}$, $\mathbf{M}_{i,j,:}^{(t+k)}$, and $\widehat{\mathbf{M}}_{i,j,:}^{(t+k)}$ are the indication matrix, ground truth tensor, and forecast tensor, respectively. $\Omega_{i,j}^{(t+k)} = 1$ if observations exist from region i to region j at step $(t+k)$; otherwise, $\Omega_{i,j}^{(t+k)} = 0$. Moreover, $\text{metric}(\cdot)$ is a generic metric function that can be any of the metrics mentioned above and defined next. For simplicity, we use \mathbf{m} and $\widehat{\mathbf{m}} \in \mathbb{R}^K$ to denote $\mathbf{M}_{i,j,:}^{(t+k)}$ and $\widehat{\mathbf{M}}_{i,j,:}^{(t+k)}$, respectively.

KL divergence,

$$\text{KL}(\mathbf{m}, \widehat{\mathbf{m}}) = \sum_{k=1}^K \widehat{m}_k \log\left(\frac{\widehat{m}_k + \delta}{m_k + \delta}\right), \quad (16)$$

where δ is a positive small value to prevent having a zero when using the \log function. We use $\delta = 0.001$ in the experiment.

Jensen-Shannon divergence,

$$\text{JS}(\mathbf{m}, \widehat{\mathbf{m}}) = \frac{\text{KL}(\mathbf{m}, \widehat{\mathbf{m}}) + \text{KL}(\widehat{\mathbf{m}}, \mathbf{m})}{2} \quad (17)$$

| Data | Model | Configuration | #Weights |
|------|-------|--|----------|
| NYC | FC | $FC_3-GRU_3^1-FC_{31,423}$ | 408,535 |
| | BF | $2 \times FC_2-GRU_2^1-FC_{2,345}$ | 391,182 |
| | BF | $2 \times GC_8^{32}-P4-GC_4^{32}-P2-GCR_2^{32 \times 4}$ | 339,726 |
| CD | FC | $FC_3-GRU_3^1-FC_{43687}$ | 567,967 |
| | BF | $2 \times FC_2-GRU_2^1-FC_{2,765}$ | 415,339 |
| | AF | $2 \times GC_8^{32}-P4-GC_4^{32}-P2-GCR_2^{32 \times 4}$ | 367,502 |

Table 2: Model Construction and Hyper-Parameter Selection

Earth mover's distance,

$$\text{EMD}(\mathbf{m}, \widehat{\mathbf{m}}) = \frac{\sum_{i=1}^K \sum_{j=1}^K F_{i,j} d_{i,j}}{\sum_{i=1}^K \sum_{j=1}^K F_{i,j}}, \quad (18)$$

where flow matrix F is the optimal flow that minimizes the overall cost from \mathbf{m} to $\widehat{\mathbf{m}}$ [31].

All three functions capture the dissimilarity between an estimated and a ground-truth distribution. Thus, low values are preferred.

6.1.5 Model Construction. The proposed frameworks are trained by minimizing the two loss functions defined in Equation 7 for BF and Equation 14 for AF, using backpropagation. We use the Adam optimizer due to its good performance. The hyper-parameters were configured manually based on the loss on a separate validation set. Specifically, we set the initialization learning rate to 0.001, set with the decay rate to 0.8 at every 5 epochs, and set the dropout rate to 0.2.

Table 2 shows the optimal configurations of the hyper-parameters for the three deep learning methods and numbers of weight parameters used in each model for both datasets. Baseline FC first encodes the input into a 2D latent space via an FC operation, denoted as FC_2 . Then it calls a GRU with 3 units and 1 layer to capture the temporal dynamics, denoted as GRU_3^1 . Finally, another FC is called to project the output from GRU to an OD stochastic tensor with the following dimensions: #Source Regions \times #Destination Regions \times #Buckets, e.g., $67 \times 67 \times 7 = 31,423$ dimensions for NYC, denoted as $FC_{31,423}$. For BF and AF, we apply two identical configurations for origin and destination factorization, which is why we have "2 \times " on the first configuration, respectively. For BF, we first utilize FC_2 to encode the input for the first factorization. Then we adopt GRU_2^1 to learn the temporal dynamics. At the end of GRU, we project the output into a corresponding factorization with the following dimensions: #Source Regions $\times r \times$ #Buckets, where r is the rank of the factorized dense matrix which we set to 5, e.g., $67 \times 5 \times 7 = 2,345$ for NYC, denoted as $FC_{2,345}$. The configuration for AF is very different from the previous two models. First, we adopt two combinations of GCNN, GC_K^Q , where Q is the filter number and K is the filter size, and pooling operation, Pp , where p is the pooling size, e.g., $GC_8^{32}-P4-GC_4^{32}-P2$ for NYC. Then, the encoded features are fed into a CNRNN with n layers where each layer has four Cheby-Nets. Assuming that the number and size of the filters are Q_c and K_c , this operation can be written as $GCR_n^{Q_c \times K_c}$, e.g., $GCR_2^{32 \times 4}$, implying 2 CNRNNs where the GCNN in each gate has 32 graph convolutional filters of size 4.

From the above configurations, although AF uses the most complex models, AF uses the fewest weight parameters (see the # weights column in Table 2).

| Data | Metric | h | NH | SVR | VAR | GP | FC | BF | AF |
|------|--------|-----|-------|-------|-------|-------|-------|-------|--------------|
| NYC | KL | 1 | 0.592 | 0.704 | 0.554 | 0.522 | 0.446 | 0.427 | 0.311 |
| | | 2 | 0.592 | 0.713 | 0.562 | 0.535 | 0.438 | 0.417 | 0.313 |
| | | 3 | 0.592 | 0.720 | 0.577 | 0.545 | 0.438 | 0.415 | 0.314 |
| | JS | 1 | 0.439 | 0.530 | 0.440 | 0.391 | 0.332 | 0.322 | 0.299 |
| | | 2 | 0.439 | 0.537 | 0.452 | 0.400 | 0.327 | 0.317 | 0.302 |
| | | 3 | 0.439 | 0.543 | 0.471 | 0.408 | 0.327 | 0.316 | 0.305 |
| | EMD | 1 | 0.293 | 0.452 | 0.305 | 0.266 | 0.250 | 0.246 | 0.214 |
| | | 2 | 0.293 | 0.455 | 0.313 | 0.270 | 0.247 | 0.243 | 0.216 |
| | | 3 | 0.293 | 0.458 | 0.317 | 0.274 | 0.247 | 0.243 | 0.217 |
| CD | KL | 1 | 0.697 | 0.818 | 0.699 | 0.674 | 0.694 | 0.582 | 0.549 |
| | | 2 | 0.709 | 0.836 | 0.715 | 0.687 | 0.689 | 0.586 | 0.555 |
| | | 3 | 0.700 | 0.822 | 0.780 | 0.684 | 0.807 | 0.792 | 0.626 |
| | JS | 1 | 0.580 | 0.672 | 0.814 | 0.597 | 0.517 | 0.438 | 0.435 |
| | | 2 | 0.584 | 0.677 | 0.869 | 0.599 | 0.513 | 0.442 | 0.444 |
| | | 3 | 0.592 | 0.692 | 0.875 | 0.619 | 0.590 | 0.571 | 0.500 |
| | EMD | 1 | 0.441 | 0.543 | 0.799 | 0.439 | 0.360 | 0.307 | 0.289 |
| | | 2 | 0.443 | 0.539 | 0.871 | 0.434 | 0.361 | 0.313 | 0.295 |
| | | 3 | 0.464 | 0.574 | 0.787 | 0.471 | 0.423 | 0.378 | 0.311 |

Table 3: Forecast Accuracy with Varying h , $s = 3$.

| Data | Metric | h | NH | SVR | VAR | GP | FC | BF | AF |
|------|--------|-----|-------|-------|-------|-------|-------|-------|--------------|
| NYC | KL | 1 | 0.592 | 0.698 | 0.566 | 0.522 | 0.453 | 0.437 | 0.343 |
| | | 2 | 0.592 | 0.706 | 0.576 | 0.535 | 0.445 | 0.421 | 0.347 |
| | | 3 | 0.593 | 0.713 | 0.587 | 0.545 | 0.440 | 0.410 | 0.348 |
| | JS | 1 | 0.440 | 0.524 | 0.442 | 0.394 | 0.337 | 0.327 | 0.305 |
| | | 2 | 0.440 | 0.531 | 0.455 | 0.404 | 0.333 | 0.318 | 0.308 |
| | | 3 | 0.440 | 0.537 | 0.472 | 0.411 | 0.331 | 0.313 | 0.310 |
| | EMD | 1 | 0.293 | 0.447 | 0.299 | 0.265 | 0.248 | 0.238 | 0.214 |
| | | 2 | 0.293 | 0.450 | 0.305 | 0.270 | 0.246 | 0.235 | 0.216 |
| | | 3 | 0.294 | 0.452 | 0.314 | 0.274 | 0.245 | 0.233 | 0.217 |
| CD | KL | 1 | 0.686 | 0.804 | 0.741 | 0.671 | 0.753 | 0.668 | 0.600 |
| | | 2 | 0.685 | 0.806 | 0.759 | 0.671 | 0.740 | 0.666 | 0.605 |
| | | 3 | 0.686 | 0.807 | 0.739 | 0.674 | 0.735 | 0.667 | 0.609 |
| | JS | 1 | 0.578 | 0.674 | 0.808 | 0.610 | 0.554 | 0.517 | 0.466 |
| | | 2 | 0.577 | 0.676 | 0.850 | 0.610 | 0.546 | 0.516 | 0.475 |
| | | 3 | 0.578 | 0.678 | 0.903 | 0.612 | 0.543 | 0.517 | 0.483 |
| | EMD | 1 | 0.449 | 0.555 | 0.716 | 0.449 | 0.394 | 0.344 | 0.304 |
| | | 2 | 0.448 | 0.557 | 0.767 | 0.448 | 0.389 | 0.344 | 0.305 |
| | | 3 | 0.448 | 0.559 | 0.890 | 0.448 | 0.386 | 0.344 | 0.306 |

Table 4: Forecast Accuracy with Varying h , $s = 6$.

6.2 Experimental Results

6.2.1 Overall Results. We compare the accuracies of the different methods, using KL, JS, and EMD to evaluate the forecast accuracy; see in Tables 3 and 4. We also vary s , i.e., the number of historical stochastic speed matrices, and h , i.e., the h -intervals ahead forecasting, to study the effect of s and h . We have the following observations. (1) The deep learning based methods perform better than the other baselines in most cases. (2) The proposed basic framework BF performs better than other methods in most settings. This indicates that the proposed frameworks, which involve factorization and RNN based forecasting, are effective for OD matrix forecasting in settings with data sparseness. (3) The advanced framework AF is significantly better than other methods, including BF, in all settings. This suggests that by taking into account the spatial correlations among regions using two GCNNs, the learned features become more meaningful, which then improves forecasting accuracy. (4) The results on NYC are better than those on CD. This is because the regions in NYC are more homogeneous (i.e., within Manhattan) than the regions in CD that cover a much larger and more diverse region. This in turn makes the traffic situations in CD much more complex and more challenging to forecast. (5) When varying h , the accuracy of AF becomes worse, i.e., larger metric values. This suggests that forecast far into the future becomes more challenge. (6) When fixing h , we compare the two tables and observe that the performance of AF is better at $s = 3$ than $s = 6$. This seems to indicate that the traffic variations are more dependent on short-term history (i.e., $s = 3$) than on long-term history (i.e., $s = 6$).

According to the above results, in the following, we only consider FC, BF, and AF, and we only consider the setting where $h = 1$ and $s = 6$, i.e., 1-step ahead forecasting with 6 historical observations.

6.2.2 Effect of Time of Day. In this experiment, we aim at investigating forecasting performance for different intervals during a day. To this end, we show the forecast accuracy across different time intervals. Figures 6, 7, and 8 show the performance on both data sets when using EMD, KL, and JS. To visualize the results across time, we aggregate the results per each 3 hours. We use three curves to represent the accuracy of FC, BF, and AF. In addition, we use bars to represent the percentages of data we have per each 3 hours. CD does not contain any data from 00:00 to 06:00, which is why the figures for CD start at 6.

Figures 6(a) and 6(b) show the accuracy based on EMD. We observe that both AF and BF outperform FC in almost all the time intervals. This suggests the effectiveness of factorization in the proposed framework when contending with data sparseness. In addition, AF has the best performance and differs clearly from FC and BF. This suggests that by further capturing spatial and spatio-temporal correlations improves the forecast accuracy.

We observe that the EMD for all the three methods is the worst in NYC during [3:00, 6:00). This is because the amount of testing data during [3:00, 6:00) is quite small, only accounting for around 1% of the total testing data. On both data sets, the best EMD values appear during [12:00, 15:00). This indicates that the traffic conditions during this time period seems to have the least dynamics thus making the forecasting less challenging. Similar trends can be observed when using KL and JS, as shown in Figures 7 and 8. Overall, the advanced framework AF achieves consistently the best forecasting performance on both datasets and on the three different evaluation metrics. More data enables more accurate forecasting.

6.2.3 Effect of Distances. In this experiment, we aim at investigating the effect of the distances between source and destination regions. We thus report the forecast accuracy with different distances. Given a source and a destination region, we use the Euclidean distance between the centroids of the two regions as its corresponding distance. We group OD region pairs based on their distances into 6 groups as shown in Figures 9, 10, and 11. We only consider OD region pairs that are below 3 km because less than 1% of the data is available for OD region pairs more than 3 km apart. Figures 9, 10, and 11 report results on EMD, KL, and JS, respectively.

Figures 9(a) and 9(b) show the EMD values at varying distances on NYC and CD, respectively. We observe that (1) BF and AF outperform FC for all distance settings and on both datasets; (2) AF outperforms BF by a clear margin. This again offers evidence of effectiveness of the proposed advanced framework and suggests that the best performance is achieved by contending the sparseness and by capturing spatio-temporal correlations. Next, when considering distances from 0.5 to 1.5, i.e., the first three points of the curves, we observe a clear descending trend in NYC, but this trend is less obvious in CD.

We also observe that curves start to increase 1 km on NYC as shown in Figure 9(a). The reason is amount of data in distance range

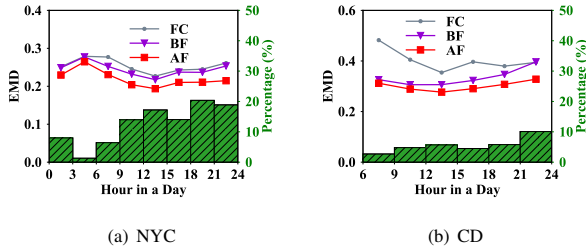


Figure 6: Effect of Time of a Day, EMD.

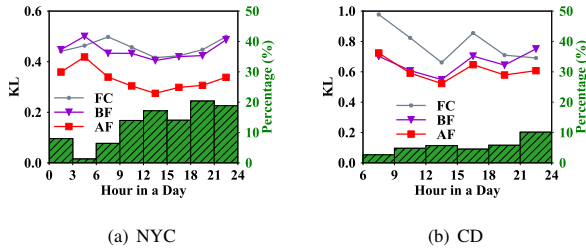


Figure 7: Effect of Time of a Day, KL.

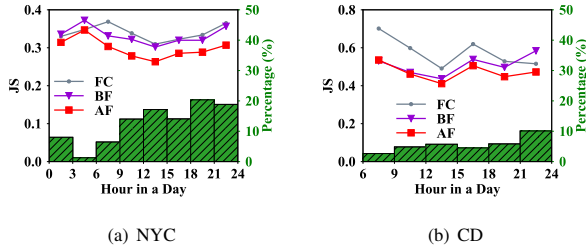


Figure 8: Effect of Time of a Day, JS.

[1.5, 3.0] decreases quickly, in turn introducing more fluctuations. We observe a subtle trend from distance range [1., 1.5] to distance range [1.5, 2.0] in Figure 9(b) for BF and AF, however, FC is much worse in distance range [1.5, 3.0]. We have similar observations for NYC regarding the KL and JS evaluation metrics, which is shown in Figures 10(a) and 11(a). The trend is much clearer in CD for the evaluation metrics of KL and JS as is shown in Figures 10(b) and 11(b). Therefore, another explanation of the increasing trend is that as the distance increases, the route options also increase, which makes the speed more stochastic and harder to forecast. Overall, AF achieves the best performance on both datasets regarding to EMD, KL, and JS evaluation metrics.

6.2.4 Effect of Proximity Matrices. We conduct a last set of experiments to investigate the effect of the parameters σ and α when constructing the proximity matrix W in the advanced framework. We only report results for CD due to the space limitation and because NYC yields similar results. Figures 12(a) and 12(b) show the accuracy when varying α and σ . The proposed AF is insensitive to σ and α . In other words, using proximity matrices is a robust way of capturing spatial correlations.

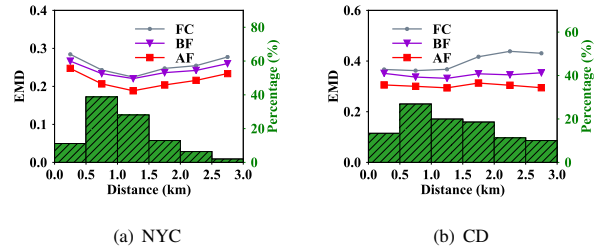


Figure 9: Effect of Distances, EMD.

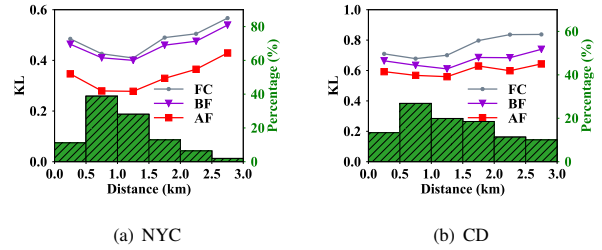


Figure 10: Effect of Distances, KL.

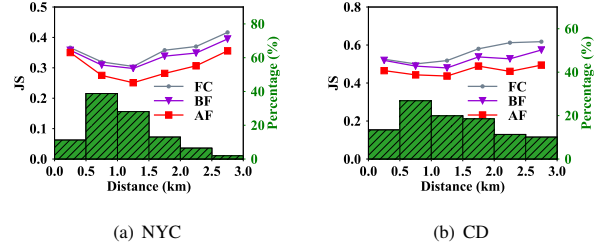


Figure 11: Effect of Distances, JS.

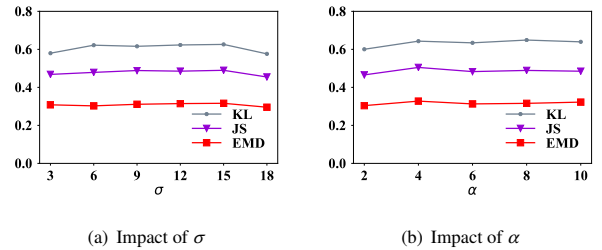


Figure 12: Results w.r.t. Hop α .

7 CONCLUSIONS AND OUTLOOK

An increasingly pertinent settings are asking for full OD matrices contain stochastic travel costs between any pair of regions in near future. However, instantiating such OD matrices calls for a large amount of vehicle trajectories which is almost an impossible task to fulfill in reality. We define and study the problem of stochastic origin-destination matrix forecasting in this setting. First, a data-driven, end-to-end deep learning framework is proposed to address the data

sparseness problem by taking advantage of matrix factorization and recurrent neural networks. Further, a dual-stage graph convolution is integrated into factorization and recurrent neural networks to better capture the spatial correlations and thus lift performance. Empirical studies on two real datasets from different countries, New York City and Chengdu City, demonstrate that the proposed framework outperforms other methods in all the experimental settings.

In future work, it is of interest to extend the framework to support continuous distribution models such as Gaussian mixture models. It is also of interest to explore distributed and parallel computing framework [48, 51] to support both the pre-processing and learning when having large amount of trajectory data.

REFERENCES

- [1] Debasish Basak, Srimanta Pal, and Dipak Chandra Patranabis. 2007. Support vector regression. *Neural Information Processing-Letters and Reviews* 11, 10 (2007), 203–224.
- [2] Joan Bruna, Wojciech Zaremba, Arthur Szlam, and Yann LeCun. 2013. Spectral Networks and Locally Connected Networks on Graphs. *arXiv:1312.6203 [cs]* (Dec. 2013). <http://arxiv.org/abs/1312.6203> arXiv: 1312.6203.
- [3] Kyunghyun Cho, Bart Van Merriënboer, Caglar Gulcehre, Dzmitry Bahdanau, Fethi Bougares, Holger Schwenk, and Yoshua Bengio. 2014. Learning phrase representations using RNN encoder-decoder for statistical machine translation. *arXiv preprint arXiv:1412.1078* (2014).
- [4] Junyoung Chung, Caglar Gulcehre, Kyunghyun Cho, and Yoshua Bengio. 2014. Empirical evaluation of gated recurrent neural networks on sequence modeling. *arXiv preprint arXiv:1412.3555* (2014).
- [5] Razvan-Gabriel Cirstea, Darius-Valer Micu, Gabriel-Marcel Muresan, Chenjuan Guo, and Bin Yang. 2018. Correlated Time Series Forecasting using Multi-Task Deep Neural Networks. In *CIKM*. 1527–1530.
- [6] Jian Dai, Bin Yang, Chenjuan Guo, and Zhiming Ding. 2015. Personalized route recommendation using big trajectory data. In *ICDE*. 543–554.
- [7] Jian Dai, Bin Yang, Chenjuan Guo, Christian S. Jensen, and Jilin Hu. 2016. Path Cost Distribution Estimation Using Trajectory Data. *PVLDB* 10, 3 (2016), 85–96.
- [8] Michaël Defferrard, Xavier Bresson, and Pierre Vandergheynst. 2016. Convolutional Neural Networks on Graphs with Fast Localized Spectral Filtering. *arXiv:1606.09375 [cs, stat]* (June 2016).
- [9] Zhiming Ding, Bin Yang, Yuanyang Chi, and Limin Guo. 2016. Enabling Smart Transportation Systems: A Parallel Spatio-Temporal Database Approach. *IEEE Trans. Computers* 65, 5 (2016), 1377–1391.
- [10] Zhiming Ding, Bin Yang, Ralf Hartmut Güting, and Yaguang Li. 2015. Network-Matched Trajectory-Based Moving-Object Database: Models and Applications. *IEEE Trans. Intelligent Transportation Systems* 16, 4 (2015), 1918–1928.
- [11] I Ekwowaksono, F Bukhari, and A Aman. 2016. Estimating Origin-Destination Matrix of Bogor City Using Gravity Model. In *IOP Conference Series: Earth and Environmental Science*, Vol. 31. IOP Publishing, 012021.
- [12] Chenjuan Guo, Christian S. Jensen, and Bin Yang. 2014. Towards Total Traffic Awareness. *SIGMOD Record* 43, 3 (2014), 18–23.
- [13] Chenjuan Guo, Yu Ma, Bin Yang, Christian S. Jensen, and Manohar Kaul. 2012. EcoMark: evaluating models of vehicular environmental impact. In *SIGSPATIAL*. 269–278.
- [14] Chenjuan Guo, Bin Yang, Ove Andersen, Christian S. Jensen, and Kristian Torp. 2015. EcoMark 2.0: empowering eco-routing with vehicular environmental models and actual vehicle fuel consumption data. *Geoinformatica* 19, 3 (2015), 567–599.
- [15] Chenjuan Guo, Bin Yang, Jilin Hu, and Christian S. Jensen. 2018. Learning to Route with Sparse Trajectory Sets. In *ICDE*. 1073–1084.
- [16] G. Hinton, L. Deng, D. Yu, G. E. Dahl, A. r Mohamed, N. Jaitly, A. Senior, V. Vanhoucke, P. Nguyen, T. N. Sainath, and B. Kingsbury. 2012. Deep Neural Networks for Acoustic Modeling in Speech Recognition: The Shared Views of Four Research Groups. *IEEE Signal Processing Magazine* 29, 6 (Nov. 2012), 82–97.
- [17] Jilin Hu, Chenjuan Guo, Bin Yang, and Christian S. Jensen. 2019. Stochastic Weight Completion for Road Networks using Graph Convolutional Networks. In *ICDE*. 12 pages.
- [18] Jilin Hu, Bin Yang, Chenjuan Guo, and Christian S. Jensen. 2018. Risk-aware path selection with time-varying, uncertain travel costs: a time series approach. *Vldb J.* 27, 2 (2018), 179–200.
- [19] Jilin Hu, Bin Yang, Christian S. Jensen, and Yu Ma. 2017. Enabling time-dependent uncertain eco-weights for road networks. *Geoinformatica* 21, 1 (2017), 57–88.
- [20] I. Jindal, Tony, Qin, X. Chen, M. Nokleby, and J. Ye. 2017. A Unified Neural Network Approach for Estimating Travel Time and Distance for a Taxi Trip. *ArXiv e-prints* (Oct. 2017). [arXiv:stat.ML/1710.04350](https://arxiv.org/abs/1710.04350)
- [21] Tung Kieu, Bin Yang, Chenjuan Guo, and Christian S. Jensen. 2018. Distinguishing Trajectories from Different Drivers using Incompletely Labeled Trajectories. In *CIKM*. 863–872.
- [22] Tung Kieu, Bin Yang, and Christian S. Jensen. 2018. Outlier Detection for Multidimensional Time Series Using Deep Neural Networks. In *MDM*. 125–134.
- [23] Thomas N. Kipf and Max Welling. 2016. Semi-Supervised Classification with Graph Convolutional Networks. *arXiv:1609.02907 [cs, stat]* (Sept. 2016). <http://arxiv.org/abs/1609.02907> arXiv: 1609.02907.
- [24] Quoc V. Le, Will Y. Zou, Serena Y. Yeung, and Andrew Y. Ng. 2011. Learning hierarchical invariant spatio-temporal features for action recognition with independent subspace analysis. In *IEEECVPR*. 3361–3368.
- [25] Yaguang Li, Kun Fu, Zheng Wang, Cyrus Shahabi, Jieping Ye, and Yan Liu. 2018. Multi-task representation learning for travel time estimation. In *International Conference on Knowledge Discovery and Data Mining (KDD)*.
- [26] Yaguang Li, Rose Yu, Cyrus Shahabi, and Yan Liu. 2018. Diffusion Convolutional Recurrent Neural Network: Data-Driven Traffic Forecasting. In *International Conference on Learning Representations (ICLR '18)*.
- [27] Benjamin M Marlin. 2004. Modeling user rating profiles for collaborative filtering. In *Advances in neural information processing systems*. 627–634.
- [28] Federico Monti, Michael M. Bronstein, and Xavier Bresson. 2017. Geometric Matrix Completion with Recurrent Multi-Graph Neural Networks. In *NIPS*. 3700–3710.
- [29] Carl Edward Rasmussen. 2004. Gaussian processes in machine learning. In *Advanced lectures on machine learning*. Springer, 63–71.
- [30] John Rice and Erik Van Zwet. 2001. A simple and effective method for predicting travel times on freeways. In *Intelligent Transportation Systems, 2001. Proceedings, 2001 IEEE*. IEEE, 227–232.
- [31] Yossi Rubner, Carlo Tomasi, and Leonidas J Guibas. 1998. A metric for distributions with applications to image databases. In *Computer Vision, 1998. Sixth International Conference on*. IEEE, 59–66.
- [32] P. Sermanet, S. Chintala, and Y. LeCun. 2012. Convolutional neural networks applied to house numbers digit classification. In *Proceedings of the 21st International Conference on Pattern Recognition*. 3288–3291.
- [33] Christopher A Sims. 1980. Macroeconomics and reality. *Econometrica: Journal of the Econometric Society* (1980), 1–48.
- [34] Nathan Srebro and Tommi Jaakkola. 2003. Weighted low-rank approximations. In *Proceedings of the 20th International Conference on Machine Learning (ICML-03)*. 720–727.
- [35] Nathan Srebro, Jason Rennie, and Tommi S Jaakkola. 2005. Maximum-margin matrix factorization. In *Advances in neural information processing systems*. 1329–1336.
- [36] Ilya Sutskever, Oriol Vinyals, and Quoc V Le. 2014. Sequence to sequence learning with neural networks. In *Advances in neural information processing systems*. 3104–3112.
- [37] Dong Wang, Wei Cao, Jian Li, and Jieping Ye. 2017. DeepSD: Supply-Demand Prediction for Online Car-Hailing Services Using Deep Neural Networks. In *33rd IEEE International Conference on Data Engineering, ICDE 2017, San Diego, CA, USA, April 19-22, 2017*. 243–254.
- [38] Dong Wang, Junbo Zhang, Wei Cao, Jian Li, and Yu Zheng. 2018. When Will You Arrive? Estimating Travel Time Based on Deep Neural Networks.
- [39] Hongjian Wang, Yu-Hsuan Kuo, Daniel Kifer, and Zhenhui Li. 2016. A Simple Baseline for Travel Time Estimation Using Large-scale Trip Data. In *Proceedings of the 24th ACM SIGSPATIAL International Conference on Advances in Geographic Information Systems (GIS '16)*. ACM, New York, NY, USA, Article 61, 4 pages.
- [40] Yilun Wang, Yu Zheng, and Yexiang Xue. 2014. Travel Time Estimation of a Path Using Sparse Trajectories. In *Proceedings of the 20th ACM SIGKDD International Conference on Knowledge Discovery and Data Mining (KDD '14)*. ACM, New York, NY, USA, 25–34.
- [41] Zheng Wang, Kun Fu, and Jieping Ye. 2018. Learning to Estimate the Travel Time. In *Proceedings of the 24th ACM SIGKDD International Conference on Knowledge Discovery & #38; Data Mining (KDD '18)*. ACM, New York, NY, USA, 858–866.
- [42] Chun-Hsin Wu, Jan-Ming Ho, and Der-Tsai Lee. 2004. Travel-time prediction with support vector regression. *IEEE Trans. Intelligent Transportation Systems* 5, 4 (2004), 276–281.
- [43] Bin Yang, Jian Dai, Chenjuan Guo, Christian S. Jensen, and Jilin Hu. 2018. PACE: a Path-Centric paradigm for stochastic path finding. *Vldb J.* 27, 2 (2018), 153–178.
- [44] Bin Yang, Chenjuan Guo, and Christian S. Jensen. 2013. Travel Cost Inference from Sparse, Spatio-Temporally Correlated Time Series Using Markov Models. *PVLDB* 6, 9 (2013), 769–780.
- [45] Bin Yang, Chenjuan Guo, Christian S. Jensen, Manohar Kaul, and Shuo Shang. 2014. Stochastic skyline route planning under time-varying uncertainty. In *ICDE*. 136–147.
- [46] Bin Yang, Chenjuan Guo, Yu Ma, and Christian S. Jensen. 2015. Toward personalized, context-aware routing. *Vldb Journal* 24, 2 (2015), 297–318.

- [47] Bin Yang, Manohar Kaul, and Christian S. Jensen. 2014. Using Incomplete Information for Complete Weight Annotation of Road Networks. *IEEE Trans. Knowl. Data Eng.* 26, 5 (2014), 1267–1279.
- [48] Bin Yang, Qiang Ma, Weining Qian, and Aoying Zhou. 2009. TRUSTER: TRjectory Data Processing on CLUSTERS. In *DASFAA*. 768–771.
- [49] Rose Yu, Yaguang Li, Cyrus Shahabi, Ugur Demiryurek, and Yan Liu. 2017. Deep Learning: A Generic Approach for Extreme Condition Traffic Forecasting. In *SIAMICDM*. 777–785.
- [50] Jing Yuan, Yu Zheng, Xing Xie, and Guangzhong Sun. 2011. Driving with knowledge from the physical world. In *SIGKDD*. 316–324.
- [51] Peisen Yuan, Chaofeng Sha, Xiaoling Wang, Bin Yang, Aoying Zhou, and Su Yang. 2010. XML Structural Similarity Search Using MapReduce. In *WAIM*. 169–181.
- [52] Hanyuan Zhang, Hao Wu, Weiwei Sun, and Baihua Zheng. 2018. DeepTravel: a Neural Network Based Travel Time Estimation Model with Auxiliary Supervision. *arXiv preprint arXiv:1802.02147* (2018).
- [53] Chenyi Zhuang and Qiang Ma. 2018. Dual Graph Convolutional Networks for Graph-Based Semi-Supervised Classification. In *Proceedings of the 2018 World Wide Web Conference on World Wide Web, WWW 2018, Lyon, France, April 23-27, 2018*. 499–508.